Mesoporous nanocarriers for the loading and stabilization of 5-aminolevulinic acid

Miletto, Ivana; Bottinelli, Emanuela; Siviero, Andrea; Fabbri, Debora; Calza, Paola; Berlier, Gloria. Mesoporous nanocarriers for the loading and stabilization of 5-aminolevulinic acid. JOURNAL OF NANOPARTICLE RESEARCH. 18 (8) pp: 1-10.
DOI: 10.1007/s11051-016-3535-6

Mesoporous Nanocarriers for the Loading and Stabilization of 5-aminolevulinic acid

Ivana Miletto[§]*, *Emanuela Bottinelli, Andrea Siviero, Debora Fabbri, Paola Calza and Gloria Berlier*

Università degli Studi di Torino, Dipartimento di Chimica, Via Pietro Giuria 7, Torino, Italy.

[§] Present address: Università del Piemonte Orientale, Dipartimento di Scienze e Innovazione Tecnologica, Viale Teresa Michel 11, Alessandria, Italy

CORRESPONDING AUTHOR:

Dr. Ivana Miletto, Università del Piemonte Orientale, Dipartimento di Scienze e Innovazione Tecnologica, Viale Teresa Michel 11, Alessandria, Italy

Tel: +39 011 360 418; E-mail: ivana.miletto@uniupo.it

ABSTRACT

Mesoporous nanoparticles bearing different surface functionalization were proposed as host carrier for the loading and stabilization of 5-aminolevulinic acid: unmodified mesoporous silica nanoparticles exposing native silanols and aminopropyltriethoxysilane grafted mesoporous silica nanoparticles exposing amino groups. The monitoring of 5-aminolevulinic acid stability over the different steps of drug loading was carried out by electronic and vibrational spectroscopies. Unmodified mesoporous nanoparticles were found to be a host system ensuring the stability of 5-aminolevulinic acid and its availability as protoporphyrin IX precursor, whilst silica surface exposing amino groups was found to strongly favour the dimerisation of 5-aminolevulinic acid to the derived compound pyrazine-2,5-dipropionic acid which is considered to be the major degradation product in aerated solutions and it is no longer active as precursor of protoporphyrin IX. This phenomenon is interpreted in term of the basic character of amino-modified silica.

Keywords: 5-aminolevulinic acid, mesoporous silica nanoparticles, drug loading, drug delivery, photodynamic therapy photosensitizer precursors

1. INTRODUCTION

5-Aminolevulinic acid (ALA, 5-amino-4-oxopentanoic acid) is a naturally occurring intermediate in the haem-synthesis pathway and is commonly used as photosensitiser precursor in photodynamic detection (PDD) and therapy (PTD) (Nokes 2013; McCarron 2008; Allison 2004). High intracellular concentrations of ALA lead to the biosynthesis of the endogenous photosensitiser protoporphyrin IX (PpIX) (Collaud 2004; Allison 2005) and the subsequent irradiation with visible light leads to singlet oxygen production and cell death through varying degrees of apoptosis and necrosis (Kennedy 1990; Li 2014).

Although ALA metabolism is mainly associated with hepatic and erythrocyte metabolism through ALA synthase (ALAS) 1 and 2, respectively, this metabolism can take place in any tissue of the human body due to the ubiquitarian presence of ALAS 1(Hunter 2011). Under normal conditions, the enzymes ALAS 1 and ferrochelatase, which is responsible for the conversion of PpIX into haem, are the two rate-limiting enzymes in haem synthesis; it is nevertheless true that exogenous ALA administration bypasses ALAS regulation and saturates ferrochelatase, thus leading to PpIX accumulation (Krammer 2008; Hryhorenko 1998). Since ALA is preferentially uptaken by cells with elevated metabolic activity, such as cancer cells, the administration of ALA results in a valid cancer-specific PTD approach.

In the last decades ALA has been successfully used in the diagnosis and treatment of various cancer and precancerous lesions, including basal cells carcinoma (Morton 1998), actinic keratosis (Jeffes 1997), Bowen's disease (Stables 1997), vulval intraepithelial and squamous cell carcinoma (MacCarron 2003; MacCarron 2004) as well as, more recently, non dermatologic organ systems, such as breast, lung, bladder, prostate, renal cancer (Millon 2010; Lam 1994; Grossman 2007; Adam 2009; Popken 1999; Hoda 2009) and central nervous system neoplasias (Eljamel 2008).

Despite ALA is a small molecule, the hydrophilic and zwitterionic character drastically limits

its permeation through skin and its diffusion through biological barriers, such as the stratum corneum (Yang 2013; Van den Akker 2000). As a consequence, an important limitation of topical ALA based PDD and PDT is that the amount of fluorescing and photosensitizing PpIX formed is limited; hence, high ALA doses have to be applied in order to achieve sufficiently high PpIX levels suitable for PDT (Cairnduff 1994; Szeimies 1994). Furthermore, the stability of ALA in non-biological, aqueous systems, such as drug delivery vehicles and formulations having pH of 6 or above, is notoriously poor and it has been evidenced to be dependent on pH, concentration, temperature and degree of oxygenation of the solution (McCarron 2005; Gadmar 2002; Novo 1995; Novo 1996). At pH values above 6 the formation of derived compounds which are no longer active as precursors of the PpIX is strongly promoted; in 1995 the pathway leading to the inactivation of ALA in solution was proposed by Novo et co-workers (Novo 1995). As shown in Scheme I, when ALA is in its anionic form the interaction between ALA molecules is favoured and deprotonation of the amino group allows cyclisation with the ketone group of the neighbouring molecule with subsequent formation of 3,6-dihydropyrazine 2,5-dipropionic acid (DHPY). Further oxidation leads to pyrazine-2,5-dipropionic acid (PY) which is considered to be the major degradation product in aerated solutions.

Scheme 1 Proposed mechanism for the dimerization of 5-ALA to DHPY and subsequent conversion to PY

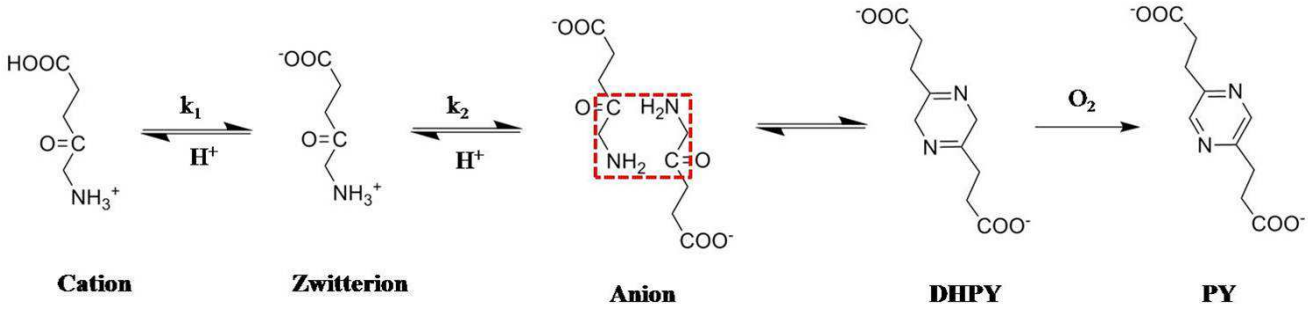

A reduction in pH enhances stability as the amino group is protonated and thus it is not readily

reactive towards cyclisation; ALA, in fact, was found to be stable over long periods when buffered at pH lower then 3, even if stored at 50°C (Elfsson 1999). This range of acidic pH, however, is not optimal for the topical administration of ALA, as the probability of cutaneous irritancy is high. It is then of outstanding importance to find new methods for the improvement of ALA stability as well as to help it pass through lipophilic barriers. The use of suitable carriers is one of the most promising approaches for improving solubilisation of drugs (Faruki 2013), protecting labile molecules (Berlier 2013; Berlier 2013; Pinto Reis 2013; Ambrogi 2007) and enhancing permeability through biological barriers (Mattheolabakis 2012). Despite porous silica based materials have been widely employed as host materials for drug delivery systems (Tripathi 2014; Zhu 2014; Kwon 2013), at the best of our knowledge only one report is present in recent literature about the use of silica based materials for ALA storage and delivery (Mottier 2011). In this work we proposed the use of MCM41 type mesoporous silica nanoparticles as host for ALA stabilization and delivery; different surface functionalizations were explored with the aim of identifying which architecture ensures the best environment for ALA hosting and stabilization.

The focus was on the physical-chemical aspects of the host-guest interaction, which were investigated by electronic and vibrational spectroscopies.

2. EXPERIMENTAL SECTION

2.1 Materials

Sodium dihydrogen phosphate monohydrate, sodium hydrogen phosphate monohydrate, sulphuric acid (96%), sodium tetraborate hydrate, hydrochloric acid (37%) and sodium hydroxide were purchased from Carlo Erba. 5-aminolaevulinic acid hydrochloride and all the other reagents and solvents were purchased from Sigma Aldrich (Italy) and used as received. Ultrapure water was produced using a Milli-QTM system (Millipore). Aqueous solutions were prepared with ultrapure water Millipore Milli-Q^{TM} (TOC < 2 ppb).

Mesoporous MCM41 type silica nanoparticles were prepared and functionalized as previously

reported (see paragraph S1 in the ESI† for details) (Miletto 2012; Radu 2004). Two different samples were prepared which differ for the surface groups exposed: *i)* non-functionalized mesoporous nanoparticles, exposing native silanol groups (hereafter *MSN*); *ii)* mesoporous nanoparticles functionalized with aminopropyltriethoxysilane, exposing amino groups (hereafter *aminoMSN*).

2.2 Methods

UV-Vis absorption spectra were recorded with a Varian CARY 100 Scan UV-Vis spectrophotometer.

2.2.1 Preparation of the ALA-MCM41 nanoparticles complexes

100 mg of *MSN*/*aminoMSN* were outgassed for 2h at 120°C and then they were added to a solution of 100 mg of ALA in 2 ml of deionized water. The suspension was stirred at 5°C for 24 h, and then the solid was recovered by centrifugation and dried at room temperature (r.t.) under vacuum for 24 h. Thermo gravimetric analyses were carried out in order to evaluate the actual ALA loading in each sample. The complexes between ALA and the two different MCM41 nanoparticles samples will be hereafter addressed at as *ALA-MSN* and *ALA-aminoMSN*.

2.2.2 Characterization of parent and ALA loaded MSN

High Resolution Transmission Electron Microscopy (HR-TEM) investigations were carried out on a JEOL 3010-UHR instrument (300 kV acceleration potential; LaB6 filament). For the measurements the MSN powders were dispersed on a copper grid coated with a perforated carbon film. The average size of MSN was obtained by measuring ca. 300 particles, and the mean particle diameter (dm) was calculated as $d_m=\Sigma d_i n_i/\Sigma n_i$, where n_i was the number of particles of diameter d_i. The result is indicated as ($d_m \pm$STDV).

Specific surface areas (SSAs) were measured by N_2 adsorption-desorption isotherms at 77K

using a Micromeritics ASAP2020 instrument. The SSA was calculated by the Brunauer-Emmet-Teller (BET) method and the average pore size according to the Barrett-Joyner-Helenda method, employing the Kruk-Jaroniec-Sarayi equations on the adsorption branch of the isotherms. Before analysis the samples were outgassed at r.t. overnight.

Powder X-ray diffraction (XRD) patterns of MSN were collected on a PANalytical X'Pert PRO instrument operating with Cu Ka radiation (1.54 Å), generated at 45 kV and 40 mA.

Thermal gravimetric analyses (TGA) were carried out on a TAQ600 (TA instruments) by heating the samples, after equilibration, from 30 to 1000°C at a rate of 10°C/min. Once the target temperature was reached, an isotherm was run for 15 min in air in order to burn carbonaceous residues from pyrolysis reactions.

Fourier Transform InfraRed spectra (FTIR) were recorded on a Jasco-6100 spectrometer equipped with a DTGS detector, working with $4cm^{-1}$ resolution over 64 scans. Samples were in form of self-supporting pellets suitable for transmission IR experiments and placed in a quartz cell equipped with KBr windows and designed for RT studies in vacuum and in controlled atmosphere. Before analysis, the samples were outgassed at RT to remove physically adsorbed water.

2.2.3 ALA derivatization for HPLC determination

Preliminary tests of ALA derivatization were performed following the procedure available in the literature (Mottier 2011). This method allows working in 0.2 M sulphuric acid, thus avoiding the degradations of substrate; modifications were applied to the original method in order to optimize the derivatization procedure. 370 ml of ALA standard solution was added to the following reagents: 400 ml of borate buffer 0.2 M dissolved whit a solution 0.1 M NaOH, 400 mL of a solution 0.1 M NaOH and 400 mL of 2.7 mM fluorescamine solution. The reaction was run for 20 min at room temperature. Linearity (quoted as R2) of calibration curves was evaluated by linear regression analysis, which was calculated by the least square regression method.

2.2.4 Release

In order to evaluate the release of ALA from *ALA-MSN* and *ALA-aminoMSN*, 2 mg of mesoporous material were suspended in 2 ml of proper solvent and stirred for 2 hours. The solvents employed were phosphate buffer (pH= 7) or HCl 0.01 M (pH=2).

The suspension was then centrifuged for 15 min at 15000 rpm and the supernatant was subjected to derivatization, following the procedure optimized as reported in paragraph 2.2.3. The quantification of ALA was performed using a HPLC Agilent 1100/1200, equipped with RP-C18 column (Lichrospher, 4 mm i.d×125 mm long, 5 μm particle size from Merck) thermostated at 25°C and a fluorescence detector, by monitoring emission at 480 nm upon excitation at 395 nm. Elution was carried out using 30/70 v/v acetate buffer (pH=3)/acetonitrile at a flow rate of 0.5 mL/min.

All experiments were run in triplicate; the data reported are the average of three replications of the release tests.

2.3 RESULTS AND DISCUSSION

2.3.1 Stability of ALA in solution

It is known by the literature that at pH<4.5 ALA aqueous solutions are stable within 6 hours, and the absorption spectrum is characterized by a component centred at 265 nm; this component could be assigned to the n→π* transition of carbonyl groups (Mottier 2011). Several studies (Gadmar 2002; Novo 1996; Elfsson 1999; Bunker 2000) underlined the instability of ALA in aqueous solution, in particular at pH> 5. The spectrum of ALA dissolved in water and basified up to pH 6 is characterized by an absorption band centred at ca.275 nm, which, according to literature (Hunter 2005), can be ascribed to the formation of PY. As mentioned before, in fact, when ALA is in its anionic form the interaction between ALA molecules is favoured and lead to the formation of cyclization products such as DHPY and PY, the latter being considered to be the major degradation compound in aerated solutions. The pH dependence of ALA degradation can be explained on the basis of the acid-base equilibria of this aminoacid: at acidic pH the

amino group of ALA is protonated so preventing the occurrence of condensation (Bunker 2000).

The extent and rate of ALA degradation also depends on its concentration and temperature. Therefore, we carried out preliminary experiments in order to identify the proper conditions for preparation, storage and analysis of the samples.

The UV-Vis spectra of ALA solutions were recorded at increasing times after their preparation, at r.t., in different milieus (water or phosphate buffer solution), at pH=2 and 7, and at concentration ranging from $1.5x10^{-4}$ to $1.5x10^{-2}$ M.

At the lowest concentration of ALA tested ($1.5x10^{-4}$ M) the spectrum showed a significant modification only after 48 h at pH = 7, with the appearance of a shoulder at 275 nm. This peak could be attributed to the formation of a dimerization product, namely PY, already observed in alkaline solutions by Granic and Mauzerall (1958).

At higher ALA concentration ($1.5 x10^{-2}$ M) at pH=7, the peak at 275 nm appears after only 1,5 hours, underlining that the ALA degradation is strongly dependent on the substrate concentration. Conversely, at pH=2 no changes in the spectrum can be seen within 48 hours after the preparation of solutions (see Figure S2-1 in the ESI†).

2.3.2 Optimization of the derivatization procedure

Due to the non-fluorescent nature of ALA, the monitoring and quantification of release via HPLC coupled with fluorescence detector is possible only upon derivatization of ALA with a fluorescence probe, such as fluorescamine. The derivatization procedure was optimized and calibration curves were plotted.

Starting from the method described by Mottier (2011), where 0.2 M sulphuric acid was employed, we tested different acids and concentrations, with the aim of obtaining an analytical procedure with increased linearity and sensibility. As already stated, previous studies on ALA pH stability showed that it is stable at pH$\leq$ 2. This allows lowering the acid concentration from 0.2 M to 0.01 M, with a gained sensibility (see Figure 1), as high concentrations of anions are

known to induce a quenching in fluorescence (Alev-Behmoaras 1979).

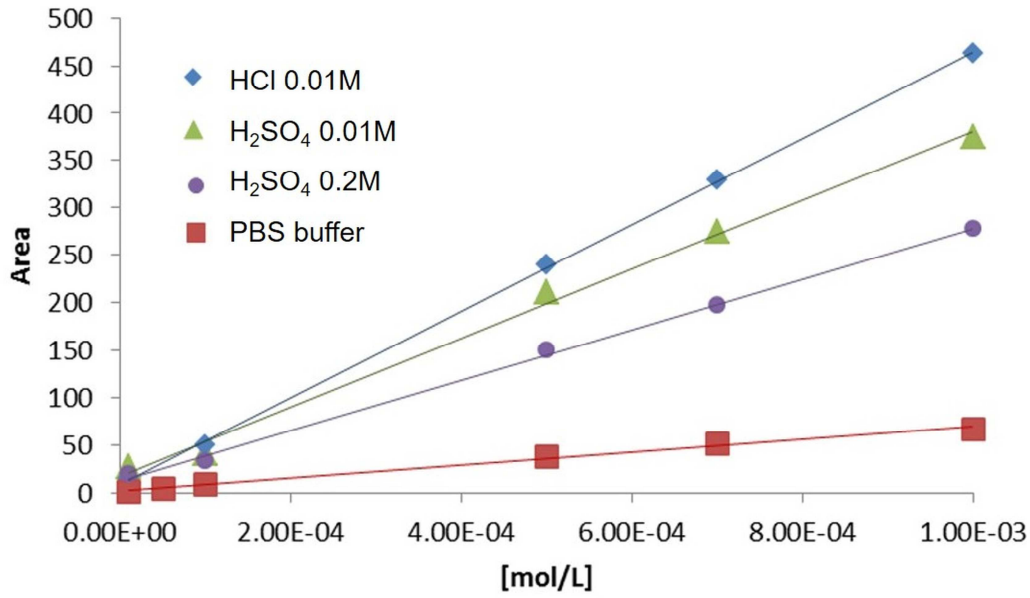

Figure 1 Calibration curve of ALA in different aqueous solutions

The influence of different anions on the fluorescence signals was also investigated; solutions of ALA were prepared at pH 2 in sulphuric acid and hydrochloric acid or at pH7 in buffer solution (phosphate buffered saline, PBS) and subsequently derivatized with fluorescamine; results are plotted in figure 1.

The highest sensibility was achieved in the presence of hydrochloric acid, whereas the slope of PBS calibration curve was the lowest. This result is in accordance with what reported in literature about the quenching effect of anion salts (phosphates) on the fluorescence of several molecules (Granick 1958).

2.3.3 Characterization of parent and ALA loaded MSN

Irrespective of the surface functionalization, the obtained materials exhibited quasi-spherical particle morphology with an average particle size of ca. 100±23 nm and regular and ordered cylindrical channels with hexagonal symmetry. In figure 2 representative HRTEM images of parent and ALA loaded MCM41 nanoparticles are reported.

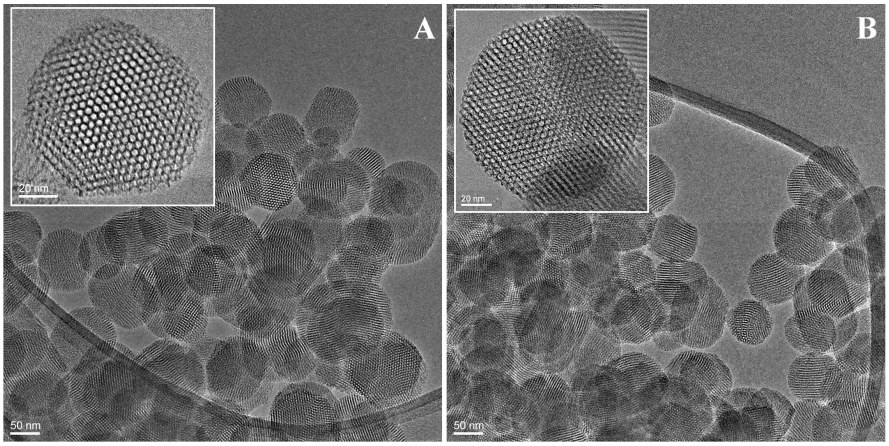

Figure 2 HRTEM images of parent (**A**) and ALA-loaded (**B**) MSN

According to the results from gas-volumetric analyses, as expected MSNs showed a type IV isotherm, typical of mesoporous materials with one-dimensional cylindrical channels (Rouquerol 1999; Kozlova 2010) and a SSA of ca. 1000 m^2/g with average pore diameter of ca. 3.4 nm, in the case of the as-synthesized material (Table 1, see figure S3-1 in the ESI† for details). A slight decrease in SSAs and average pore diameters were detected in the case of the functionalized materials. The loading of ALA caused a decrease of textural properties in both cases, but in a quite drastic amount in *ALA-aminoMSN* complex. The maintenance of the regular mesoporous structure after functionalization and loading was assessed also by HRTEM and XRD analysis (see figure S3-2 and S3-3 in the ESI† for details).

Table 1 Volumetric data of parent MSN and derived drug-complexes

Sample	Volumetric data		
	SSA (m^2/g)	Cumulative Pore Volume (cm^3/g)	Average Pore diameter (nm)
MSN	1011	1.68	3.4
aminoMSN	920	1.23	2.7
ALA-MSN	879	0.43	3.2
ALA-aminoMSN	~ 90	~ 0.27	2.3

Actual loading values, evaluated by thermo gravimetric analysis, are reported in table 2, along with the release values, analysed by HPLC. The obtained loadings were found not to be severely

dependent on the functionalization of the mesoporous carrier and were found to be around 10 wt%. This value is interestingly higher than the 3.4% wt% loading obtained by Ma and co-worker (2015) in the case of loading of ALA in hollow mesoporous systems.

The release tests were carried out in two different environments: PBS buffer (pH 7) and hydrochloric acid solution at pH=2. The 65% and 73% of the loaded drug was released in PBS from the *ALA-MSN* and *ALA*-aminoMSN, respectively. Conversely, the extraction efficiency of hydrochloric acid is low: approximately the 27% of the loaded ALA is released from *ALA-MSN* complex and only the 25% of the loaded drug is released from the complex in the case of the amino-functionalised nanoparticles.

Table 2 Loading and release data

Sample	Loading w/w* %	Release			
		PBS (pH=7)		HCl (pH=2)	
		g	w/w* %	g	w/w* %
ALA-MSN	10.0	$1.3x10^{-4}\pm7.8x10^{-6}$	6.5	$7.9x10^{-5}\pm3.9x10^{-6}$	2.69
ALA-aminoMSN	9.7	$1.4x10^{-4}\pm7.7x10^{-6}$	7.1	$3.5x10^{-5}\pm2.0x10^{-6}$	1.75

* weight of 5ALA per weight of complex

In order to monitor the stability and integrity of ALA during the preparation of the complexes, UV-Vis measurement on the ALA solutions and on the supernatants after the loading procedures were carried out. Furthermore, the complexes *ALA-MCM41 nanoparticles* were characterized by DR-UV-Vis and FT-IR spectroscopy in order to assess the integrity of the ALA within the pores of MCM41 nanoparticles and to investigate the drug-carrier interactions, respectively.

In order to exclude any influence of the mesoporous host on the pH of the loading solutions, pH of the distilled water used in this experiments and of the MCM41 nanoparticles suspensions were measured. The registered values are reported in table 3, along with the pH values measured on the ALA water solution and on the supernatants after the loading step.

Irrespective of the functionalization, the presence of MSN was found not to have significant influence on the pH of the aqueous solution, which was always approximately 6.7-6.8. The pH of the loading suspensions was the same of the supernatants collected after the complexation step, and it was slightly different as a function of the functionalization but always in a pH range which ensure the stability of ALA.

Table 3 pH values measured

	pH
water	6.71
5-ALA in water	1.91
MSN in water	6.68
aminoMSN in water	6.85
ALA-MSN in water – SUPERNATANT*	1.97*
ALA-aminoMSN in water – SUPERNATANT*	3.78*

* the pH value measured on the supernatant was the same measured on the suspension during the loading procedure

The absorption spectra of the supernatants (figure 3A) are characterized by the same component at 265 nm as for the ALA solution in water; this result suggests that the choice of deionized water at acid conditions as solvent ensures a good control on the stability of the drug during the loading procedure, which was not achieved when ethanol was used. In fact, ALA was found not to be stable in ethanol, as the pH of the ALA solution and of the supernatants was around 5.8 and absorption spectra clearly evidenced the formation of dimers (peak at 275 nm ascribable to PY)[see figure S4-1 in the ESI† for further information].

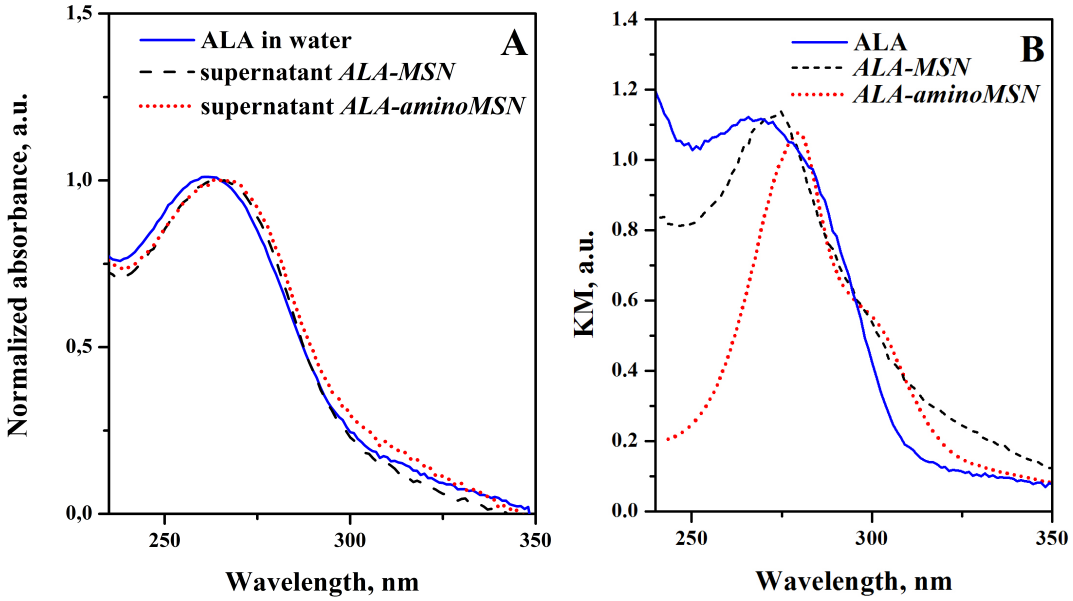

Figure 3 A) UV-Vis absorption spectra of ALA in water (blue-solid line) and supernatant after loading of *ALA-MSN* (black-dashed line) and *ALA-aminoMSN* (red-dotted line); B) DR-UV-Vis spectra of ALA (blue-solid line) and complexes *ALA-MSN* (black-dashed line) and *ALA-aminoMSN* (red-dotted line)

Despite the spectra acquired on the supernatants showed that ALA stability was ensured in the loading environment, the DR-UV-Vis revealed that in the case of *aminoMSN* the surface features of the mesoporous silica promoted the formation of dimerization/degradation compounds that are no longer active for PDT applications. As it can be seen in figure 3B, DR-UV-Vis spectrum measured on the *ALA-MSN* sample is characterised by a single main component centred at ca. 270 nm, which can be ascribed to the n→π* transition of carbonyl groups of ALA which is red-shifted with respect of what found in solution due to the interaction with the silica surface (Viseu 2003). Conversely, the spectra of the *ALA-aminoMSN* sample present absorption features centred at 275 nm, compatible with the presence of dimers or degradation compounds.

In order to have a better insight into the structural integrity of ALA when in interaction with the

silica surface of non-functionalised and functionalised MSN, a FT-IR study was carried out. In figure 4 the infrared spectra of various *ALA-MCM41 nanoparticles* complexes are reported (curve a refers to *ALA-MSN* and curve c refers to *ALA-aminoMSN*) and compared to the spectra of the unloaded inorganic matrices (curve b refers to *MSN* and curve d refers to *aminoMSN*) and of the ALA itself (curve e in figure 4; see paragraph S5 in the ESI† for the detailed infrared spectroscopy characterization of ALA). At high frequency (figure 4, section A) the infrared spectra of both the parent and the complexed MSN are dominated by the broad absorption centred at 3500 cm^{-1} due to stretching of Si-OH groups involved in hydrogen-bonding together with hydroxyl groups of adsorbed water (Braschi 2012). In the complexes, the OH stretching signal of isolated surface silanols that can be observed at 3745 cm^{-1} on parent MSNs decreases in intensity, thus indicating that they are involved in the interaction with carboxylic, ketone and amino groups of ALA.

Due to the broad O-H stretching band mentioned before, it is not easy to clearly identify all the signals of 5-ALA in this region. Signals due to symmetric and antisymmetric stretching of NH_3^+ groups which can be found in the 3000-3100 cm^{-1} range in the FTIR spectrum of ALA (curve e), as well as the complex pattern expected in the 2400-2800 cm^{-1} range due to combination mode of C-O stretching and O-H deformation (Chen 2003), are barely visible in the FTIR spectrum of the ALA-MSN complex. In the case of *ALA-aminoMSN* the signals in the same region are not easily ascribable to the drug, as the carrier itself is bearing analogue signals, being functionalized with aminopropylic chains.

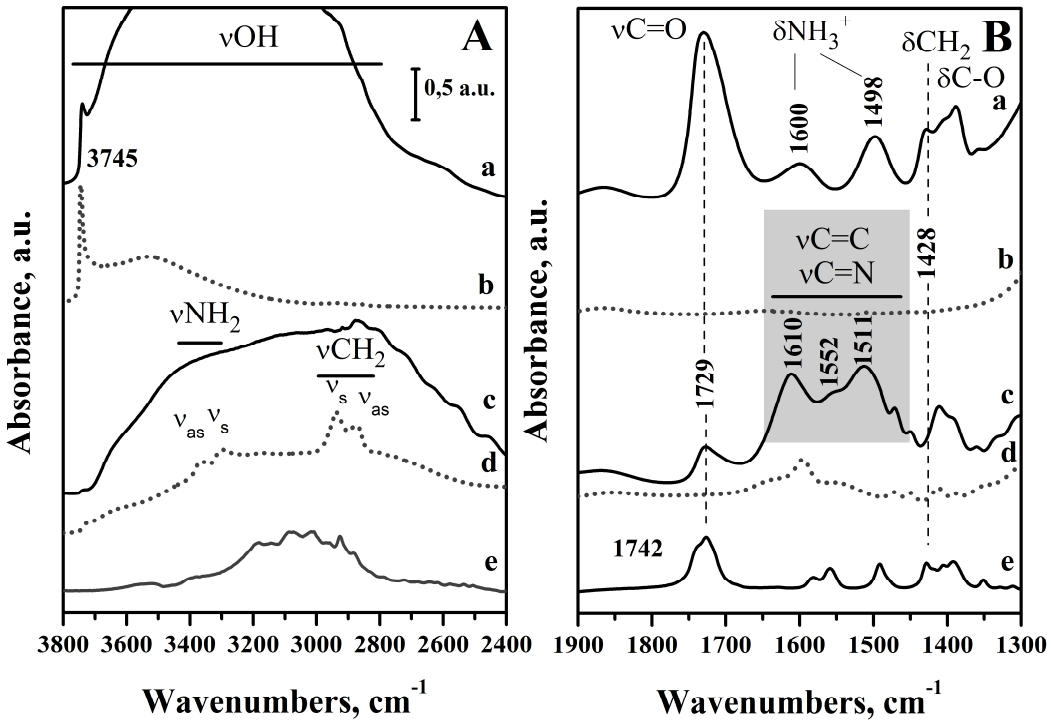

Figure 4 FTIR spectra of *ALA-MSN* (curve a) and *ALA-aminoMSN* (curve c) complexes, of the corresponding un-loaded materials *MSN* (curve b) and *aminoMSN* (curve d) and of ALA in KBr (curve e). A) High frequencies range; B) Low frequencies range.

The low frequency range (figure 4, section B) provides more interesting insights into the drug-carrier interactions that take place in the different complexes. In the infrared spectrum of the *ALA-MSN* complex the signal at 1729 cm^{-1} is assigned to C=O stretching of the ketone group of ALA; the breadth and asymmetry of the signal suggest the possible contribution of the C=O stretching of the carboxylic acid group to this band, component which is clearly visible in the spectrum of ALA diluted in KBr. Signals ascribable to the antisymmetric and symmetric modes of NH_3^+ groups are expected to be in the 1660-1590 cm^{-1} and 1550-1486 cm^{-1} range respectively; on such a basis the components at 1585-1560 cm^{-1} and the broad band at 1600 cm^{-1} in the spectra of ALA itself and of the *ALA-MSN* complex respectively were assigned to $\delta_{as}NH_3$ and the band found at 1492 cm^{-1} in the spectrum of ALA and at 1498 cm^{-1} in the spectrum of the complex to δ_sNH_3. Additional signals, due to bending modes of CH_2 (1428 and 1402 cm^{-1}) and

C-O bond (1390 cm^{-1}) of ALA, are present.

In the case of the *ALA-aminoMSN* complex, the modification induced to the infrared pattern of ALA in the low frequencies region is more severe. The stretching band of C=O bond is less intense, more broad and highly asymmetric and a new set of signals in the 1680-1470 cm^{-1} range arises, with main components centred at 1610, 1552 and 1513 cm^{-1}. These frequencies are typical for aromatic ring vibrations (C=C and C=N stretching in aromatic rings) and fully compatible with the hypothesis drawn before about the formation of PY when ALA is loaded within *aminoMSN*. This phenomenon could be ascribed to the protonation of the aminopropyl groups of silica (Tataurova 2012; Rosenholm 2008) competing with the cationic/zwitterionic form of ALA. This could favour the formation of anion species, which can then dimerize. This interpretation is supported by the increase in pH observed in the corresponding supernatant, with respect to the pH measured in ALA solution and *ALA-MSN* supernatant.

2.4 CONCLUSIONS

Mesoporous nanoparticles bearing different surface functionalization were proposed as host carrier for the loading and stabilization of ALA. Two different surface features were explored: native silanol groups exposed by unmodified mesoporous nanoparticles and amino groups exposed by mesoporous nanoparticles modified via grafting with aminopropyltriethoxysilane. Water was found to be a good solvent for the loading procedure, without any adjustment of pH needed, as ALA was stable in the loading environment irrespective of the functionalization borne by the mesoporous nanoparticles employed as host. Unmodified mesoporous nanoparticles were found to be a host system ensuring the stability of ALA and its availability as PpIX precursor. Silica surfaces exposing amino groups were found to strongly favour the dimerisation of ALA to the derived compound pyrazine-2,5-dipropionic acid which is considered to be the major degradation product in aerated solutions and it is no longer active as precursor of PpIX.

Acknowledgments

Compagnia di San Paolo and University of Turin are gratefully acknowledged for funding Project ORTO114XNH through ‘‘Bando per il finanziamento di progetti di ricerca di Ateneo - anno 2011”. This work was supported by the European COST Action MP1202 “Rational design of hybrid organic inorganic interfaces: the next step towards advanced functional materials”.

† Electronic Supplementary Information (ESI) available: [*MSN* and *amino-MSN* preparation and characterization details; UV-Vis absorption spectra of ALA as a function of pH and time, UV-Vis absorption spectra of ALA in ethanol, detailed FTIR characterization of ALA].

REFERENCES

Adam C., Salomon G. et al. (2009) Photodynamic Diagnosis Using 5-Aminolevulinic Acid for the Detection of Positive Surgical Margins during Radical Prostatectomy in Patients with Carcinoma of the Prostate: A Multicentre, Prospective, Phase 2 Trial of a Diagnostic Procedure. Eur. Urol. 55:1281-1288

Alev-Behmoaras T., Toulme J., Hélène C. (1979) Quenching of tyrosine fluorescence by phosphate ions: a model study for protein-nucleic acid complexes. Photochem. Photobiol. 30:533–539

Allison R.R., Mota H.C., Sibata C.H. (2004) Clinical PD/PDT in North America: an historical review. Photodiagn. Photodyn. Ther. 1: 263-277.

Allison R.R., Cuenca R. et al. (2005) PD/PDT for gynecological disease: a clinical review. Photodiagn. Photodyn. Ther. 2: 51-63

Ambrogi V., Perioli L., Marmottini F., Latterini L., Rossi C., Costantino U. (2007) Mesoporous silicate MCM-41 containing organic ultraviolet ray absorbents: Preparation, photostability and in vitro release. J. Phys. Chem. Solids. 68: 1173-1177

Berlier G., Gastaldi L., Ugazio E., Miletto I., Iliade P., Sapino S. (2013) J.Colloid Interf. Sci. 393: 109-118

Berlier G., Gastaldi L., Sapino S., Miletto I., Bottinelli E., Dichirio D., Ugazio E. (2013) Int. J. Pharm. 457: 177-186

Braschi I., Gatti G., Bisio C., Berlier G., Sacchetto V., Cossi M., Marchese L. (2012) J.Phys.Chem C. 116: 6943-6952.

Bunker A., Zerbe O., Schmid H., Burmeister G., Merkle H. P., Gander B. (2000) J. Pharm. Sci. 8:1335-1341.

Cairnduff F., Springer M., Hudson E.J., Ash D.V., Brown S.B. (1994) Br. J. Cancer 69:605-608

Chen J.Y., Peng Q., Jodl H.I. (2003) Spectrochimica Acta Part A. 59:2571-2576

Collaud S., Juzeniene A., Moan J., Lange N. (2004) Curr. Med. Chem.-Anti Cancer Agents 4: 301-316

Elfsson B., Wallin I., Eksborg S., Rudaeus K., Ros A.M., Ehrsson H. (1999) Eur. J. Pharm. Sci.7:87-91

Eljamel M.S., Goodman C., Moseley H. (2008) Lasers Med. Sci. 23:361-367

Faruki Md.Z., Rishikesh, Razzaque E., Bhuiyan M.A. (2013) JPSR. 4: 1569-1574

Gadmar O.B., Moan J., Scheie E., Ma L.W., Peng Q. (2002) J.Photochem. Photobiol. B-Biol. 67:187-193

Granick S. and Mauzerall D. (1958) J. Biol. Chem.232:1119-1140.

Grossman H.B.(2007) J. Environ. Pathol. Toxicol. Oncol. 26: 143-147

Hoda M.R., Popken G. (2009) J. Surg. Res.154: 220-225

Hryhorenko E.A., Oseroff A.R., Morgan J., Rittenhouse-Diakun K. (1998) Immunopharmacology 40: 231-240

Hunter G. A., Rivera E., Ferreira G. C. (2005) Arch. Biochem. Biophys. 437:128-137.

Hunter G.A., Ferreira G.C. (2011) Biochim. Biophys. Acta 1814: 1467-1473

Jeffes E.W., McCullough J.L. et al. (1997) Arch. Dermatol. 133: 727-732

Kennedy J., Pottier R., Pross D.(1990) J. Photochem. Photobiol. B 6: 143-148

Krammer B., Plaetzer K. (2008) Photochem. Photobiol. Sci. 7: 283-289

Kaliszewski M., Kwasny M., Kaminski J., Dabrowski Z., Burdziakowska E. (2004) Acta Poloniae Pharm. 61:15-19.

Kozlova S.A., Kirik S.D.(2010) Micropor. Mesopor. Mater. 133, 124-133

Kwon S., Singh R.K., Perez R.A., Abou Neel E.A., Kim H-W., Chrzanowski W. (2013) J. Tissue Eng. 4:1-19

Lam S..(1994) Semin. Oncol. 21: 15-19

Li X., Zou Z.P., Hu L., Zhang W.J., Li W.(2014) J. Dermatolog. Treat. 25: 428-433

Ma X., Qu Q., Zhao Y. (2015) ACS Appl. Mater. Interfaces, 7 (20): 10671–10676

MacCarron P.A., Donnelly R.F., Woolfson A.D., Zawislak A., Price J.H., Maxwell P.(2004) Br. J. Dermatol. 151(68): 105-106

MacCarron P.A., Donnelly R.F., Woolfson A.D., Zawislak A. (2003) Drug Deliv. Sys. Sci. 3: 59-64

McCarron P.A., Donnelly R.F., Andrews G.P., Woolfson A.D. (2005) J. Pharmac.Sci. 94(8): 1756-1771

McCarron P.A., Donnelly R.F., Woolfson A.D. (2008) Pharmaceutical Research, 25(4): 812-826

Mattheolabakis G., Rigas B., Constantinides P.P. (2012) Nanomedicine 7: 1577-1590

Miletto I., Bottinelli E., Caputo G., Coluccia S., Gianotti E. (2012) Phys. Chem. Chem. Phys. 14: 10015-10021

Mottier N., Jeanneret F.(2011) Evaluation of two derivatization reagents for the determination by LC-MS/MS of ammonia in cigarette mainstream smoke. J. Agric. Food Chem. 59:92-97

Millon S.R., Ostrander J.H., Yazdanfar S., Brown J. Q., Bender J. E., Rajeha A., Ramanujam N. (2010) J. Biomed. Opt. 15: 018002

Morton C.A., MacKie R.M., Whitehurst C., Moore J.V., McColl J.H. (1998) Arch. Dermatol.134: 248-249

Nokes B, Apel M, Jones C, Brown G, Lang J.E.(2013) Journal of Surgical Research, 181: 262-271

Novo M., Huttmann G., Diddens H.(1995) Society of Photo-Optical Instrumentation Engineers 2371:204-209

Novo M., Huttman G., Diddens H (1996). J. Photochem. Photobiol. B-Biol. 34:143-148

Pinto Reis C., Silva C., Martinho N., Rosado C. (2013) Therapeutic delivery. 4: 251-265

Popken G., Wetterauer U., Schultze-Seemann W.(1999) BJU Int. 83: 578-582

Radu D. R., Lai C.-Y., Jeftinija K., Rowe E. W., Jeftinija S., Lin V.S.Y. (2004) J. Am. Chem. Soc. 126: 13216-13217

Rosenholm J.M., Lindén M.(2008) J. Contr. Release. 2008, 128: 157-164

Rouquerol F., Rouquerol J., Sing K. (1999) Adsorption by Powders & Porous Solids, Academic Press

Stables G.I., Stringer M.R., Robinson D.J., Ash D.V. (1997) Br. J. Dermatol. 136: 957-960

Szeimies R-M., Sassy T., Landthaler M. (1994) Photochem. Photobiol. 59:73-76

Tataurova Y., Sealy M.J., Larsen R.G., Larsen S. (2012) J. Phys. Chem. Lett. 3: 425-429

Tripathi R., Verma S., Easwari T.S., Shukla V.K. (2014) Int.J.Pharm.Res.Scholars 3: 214-234

Van den Akker J.T.H.M, Iani V., Star W.M., Sterenborg H.J.C.M., Moan J. (2000) Photochem. Photobiol. 72(5):681-689

Viseu T.M.R., Hungerford G., Coelho A.F., Ferreira M.I.C.(2003) J. Phys. Chem. B. 107: 13300-13312

Yang S-J., Lin C-F., Kuo M-L., Tan C-T. (2013) Biomacromolecules 14:3183-3191

Zhu C-L., Wang X-W., Lin Z-Z., Xie Z-H., Wang X-R. (2014) J. Food. Drug Anal. 22:18-28